High resolution surface contact temperature measurements by means of micro-thermocouples in vacuum conditions

L. Thiery*, J.Y. Rauch and Y. Lei.
Université de Franche-Comté, CNRS, institut FEMTO-ST, F-25000 Besançon, France

Abstract: we report on the possibility to measure the temperature of micro-devices in vacuum conditions by means of micro-thermocouples. The principle is similar to point contact probing in Scanning Thermal Microscopy (SThM) and requires a rigorous calibration procedure to eliminate measurement errors due to surface-to-sensor heat transfer. A thin platinum wire is used as a hot wire calibration specimen and two micro-thermocouples are tested. An example of measurement is shown on a metallized fibre tip used as an optically driven thermal actuator.

Keywords: temperature measurement, micro-thermocouple, contact surface temperature, vacuum, calibration.

1. Introduction

Surface temperature measurement with high spatial resolution remains a major issue since none of the current techniques are mature enough to provide reliable measurements. Available techniques can be classified in two groups: conventional (far-field or non-contact) and local (near-field or contact). However, for both groups, major uncertainties and drawbacks rely on the physics principle of the technique but also on the heat transfer that relate the sample to the thermal detector. Non-contact techniques are typical conventional techniques which are not subjected to the aforementioned uncertainties but are limited in terms of spatial resolution, temperature range and their dependence on the surface optical nature. These encompass optical techniques such as infrared or near-infrared thermography [1,2], thermoreflectance [3,4,5], photoluminescence [6] or Raman spectroscopy [7,8]. Luminescent thermometry can however reached the nanometer resolution when using nanoparticles as distributed tracers on a surface but the technique remains complicated to implement [9]. These nanoparticles can be used individually as a single tracer on a tip to perform a local probe for contact techniques. As any local probe principle, part of these drawbacks is solved but heat transfer between the sample and the sensor becomes the main error source that needs to be carefully addressed. Among available techniques, liquid crystal thermography [10], fluorescence thermography [11] or near-field optical thermography (NFOT) [12] are also based on an optical measurement. Thermal local probing techniques are generally called Scanning Thermal Microscopes (SThM). Progress in manufacturing thermal probes at the very tip of tapered materials have led to a family very closed to Atomic Force Microscope (AFM) for which a thermal sensitive area provides an additional information related to heat transfer between this area and the sample. Thermocouple, thermodiode and more recently SQUID sensors [13] allow a quasi-punctual measurement while thermoresistive elements provide an integrated temperature value. These sensors are used to measure temperature distribution on hot samples (passive mode) or sample thermal properties when an additional heat source causes a heat transfer between the probe and the sample. In any case, quantitative measurements remain hard to derive and represent a challenge [14-16]. The last point to clarify is the available temperature range of the probe. Thermoresistive wire element such as Wollaston 5 micrometers in diameter platinum-rhodium wire probe is probably the most robust [17]. Otherwise, thin-film microfabricated probes cannot exceed a hundred degrees typically except micro-pipette thermocouple for which the temperature limit is about 500°C [18]. For years, many attempts to develop micrometric size thermocouple or thermodiode sensors have been proposed by authors from the welding of K type wires [19], S types [20,21], thin-film deposition on a micropipette [18], to an AFM [22,23] or cantilever structured [24,25] or optical fiber tip [26]. In this article, we present the use of wire thermocouple probes to measure contact temperature at micron-scale in a vacuum chamber of a Scanning Electron Microscope (SEM) coupled to a Focused ion Beam (FIB). Micron-size wire thermocouple represents a interesting compromise between their facility to implement, their robustness and their temperature range. A specific calibration procedure is described for vacuum measurement and an example of temperature measurements on a tapered metallized optical fibre is presented.

2. Micro-thermocouple probes

Thin wire thermocouples, so-called microthermocouples, are made with wires whose diameters are typically below 50 µm. They are used in a very few laboratories since it remains a challenge to produce them. Indeed, the thinnest can be obtained by welding two S-type Wollaston wires (Pt and Pt-10%Rh) of various diameters. Among available diameters, the most attractive are 5 µm and 1.3 µm since they represent the best compromise between size and robustness. The silver cladding around Pt or Pt-Rh core (diameter about 75 µm) is removed by chemical (nitric acid) or electro-chemical etching process [27]. We have extensively used such micrometric thermocouples in different applications [28] and in

* corresponding author: laurent.thiery@univ-fcomte.fr

spite of their fragility they remain an ideal means for temperature measurement on microsystems in a large temperature range. More recently, they have been integrated on a quartz tuning fork to control the force when a contact between the tip and a sample occurs [29]. As a result, they are also used as Scanning Thermal Microscope (SThM) probes for both passive and active local sensors [30,31]. For that purpose, the thermocouple junctions are systematically reshaped by means of a focused ion beam (FIB) in order to refine the tip apex and optimize the probe spatial resolution. An example of junction reshaping result is presented in Fig. 1.

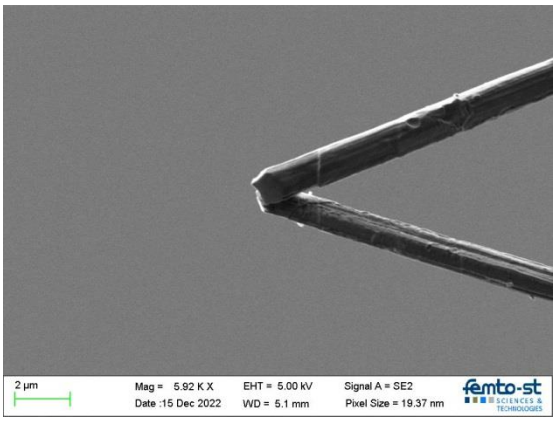

Fig. 1. Thermocouple junction obtained with 1.3 µm wire diameters after reshaping by FIB.

3. Thermal contact of a temperature probe problem

Measuring a temperature by means of a contact probe is a hard task when the probe size is not negligible regarding the tested device itself. Discrepancies are not only derived from the probe accuracy itself, but from disturbances involved in the probe to device heat balance. This problem has been addressed a long time ago for macroscopic measurements [32,33]. It is also critical in Scanning Thermal Microscopy (SThM) and requires continuous efforts to solve it. The direct approach consists in a passive measurement called "temperature contrast mode" (TCM). This is the simplest way but needs to perform a thorough calibration procedure as presented in this article. The other way consists in active measurements by heating the probe in order to cancel the dissipative heat between the sample and the probe. Such an active mode, also called "conductivity contrast mode" (CCM), has been proposed in the null-point and the double-scan techniques [34,35] for temperature measurements. These techniques are very similar, nevertheless, even if recent improvements led to reduce their complexity, they remain very difficult to implement and suffer from limitations [36,37]. The most critical one relies on the conception of commercially available probes which are very compact, very fragile and cannot be moved in any direction of space. Furthermore, only flat samples can be tested so that there is no possibility for these probes to be used in the present situation of 3D micrometre to millimetre size devices. As a result, more classical thermal probes are the best alternative especially if the tested device is a complex structure. A compromise between the flexibility of use and a lower resolution leads to the use of micron-size thermocouple for micron-scale thermometry in passive mode as a relevant mean. About vacuum temperature measurements, they are more difficult than in ambient conditions due to the suppression of the convection heat transfer, reducing the diffusion of heat between the surface and the probe, as well as the difficulty of accessing the vacuum chamber. As far as we know and except the specific case of SThM, most of vacuum temperature measurements rely on space environment applications for which thermocouples and fibre sensors (Raman scattering or Bragg grating) are generally used. In these cases, the sensitive part of the sensors is firmly attached on the surface so that the measured temperature is assumed to be the actual surface temperature [38]. In the present work, the use of a micro-thermocouple similar to SThM probes for point to point operating mode remains the only means to preserve the spatial resolution that could not be reached with infrared method for instance and allowing to be moved in all directions in a vacuum chamber. However, since a passive method has been chosen, a thorough calibration protocol is necessary prior to any measurement in order to quantify the errors that stem from such a contact measurement. Indeed, when the thermocouple junction is put in contact with a hot device, some thermal effects occur. To address the problem, the general thermal scheme consists in a quite simple approach of thermal resistances identification: R_c, R_e et R_m, for contact, external and macro-constriction – or spreading – respectively [30]. The configuration and thermal effects involved in the tip-to-sample contact is depicted in Fig. 2.

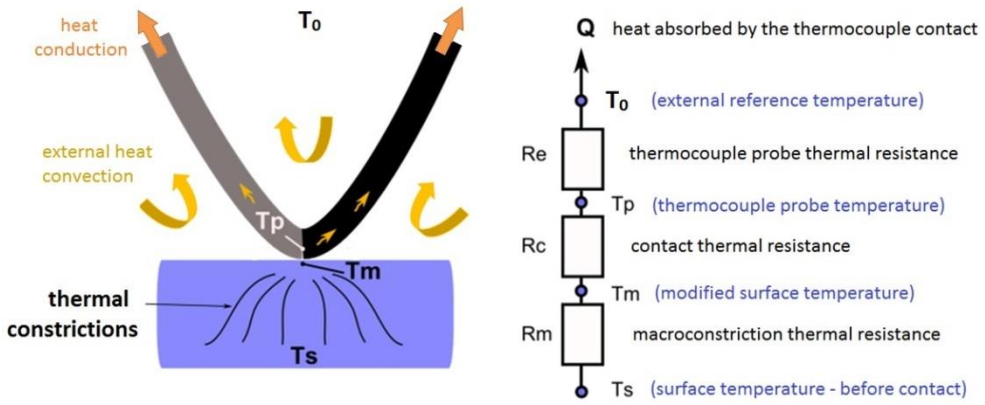

Fig. 2. Thermal phenomena involved in a thermocouple tip-to-sample contact.

The thermocouple acts as a heat sink, whose power Q is dissipated from the contact area to the probe leads through the thermocouple wires. This heat is extracted from the hot device at the contact point through the different resistances from the initial surface temperature T_s (before contact) to the cold reference one T_0, following:

$$Q = \frac{T_s - T_0}{R_m + R_c + R_e} = \frac{T_m - T_p}{R_c} = \frac{T_p - T_0}{R_e} = \frac{T_s - T_m}{R_m} \qquad (1)$$

Here, T_m is the point contact temperature underneath the probe (modified temperature) and T_p is the value given by the probe. The final goal is to deduce T_s before contact from the measured value T_p during contact. The correction to apply is called "thermal response" of the probe τ given by the ratio:

$$\tau = \frac{R_e}{R_m + R_c + R_e} = \frac{T_p - T_0}{T_s - T_0} \qquad (2)$$

For a perfect probe, T_p equals T_s and the thermal response equals 1.
This never happens and depending on the device on which the thermocouple has to be put, different phenomena may occur. Indeed, realistic cases of contacting a probe onto a sample take place between two limits:

- An ideal situation for which R_e tends to infinity or Q is negligible. This also corresponds to a negligible macroconstriction resistance R_m when the sample cannot be perturbed; either this sample is massive in size or a large amount of heat compensates the dissipation heat Q. As a result, the surface temperature before contact T_s remains unchanged and T_m equals T_s.
- Huge disturbance of the probe during contact when R_e is low. This also corresponds to an important macroconstriction resistance R_m of a very tiny sample and/or a very low available heat power regarding the dissipated heat Q. As a result, T_m is very different from T_s. This will be the practical case of the present work.

In the following, we use a thin platinum wire (diameter 5 µm) that possibly represents some micro-device to be tested in the SEM chamber. Furthermore, it is very simple to adjust the input power and measure its own temperature before and during contact as it will be shown in the theoretical model. Indeed, it is heated by Joule effect, and as a hot wire sensor, its temperature is deduced from its electrical resistance. A calibration protocol has been designed for extracting the different thermal resistances and the thermal response to be applied under vacuum.

4. Vacuum wire model

Nomenclature : wire parameters
d: diameter (m)
L: half-length (m)
s: cross section (m^2)
x: longitudinal coordinate along the wire (m)
i: current (A)
ρ_{el}: electrical resistivity (Ω.m)
α: temperature coefficient of resistance (K^{-1})
k: thermal conductivity ($W.m^{-1}.K^{-1}$)

Let us consider a cylindrical wire of L half-length and d diameter. The axis origin (x=0) is the centre location so that the total length is 2×L. Due to a very low diameter (5 µm), a section is thermally homogeneous so that the temperature distribution only depends on the longitudinal direction x. Each wire extremity (x = ± L) is welded to a large copper lead which maintains the local temperature as a constant initial value, T_0.

The used micro-thermocouple is put in contact with the wire at the origin x = 0, central location where the wire temperature is maximum. When the contact occurs, a heat sink is generated through a thermal conductance "g" to a cold source at the same temperature T_0 which is the thermocouple cold junction reference.

In the following, only the temperature difference θ will be considered regarding the reference value T_0, generally identical to ambient so that: $\theta = T - T_0$.

This value is measured by means of a Pt100 sensor located on the copper lead. The temperature distribution along the wire is governed by the solution of the fin differential equation obtained from the thermal balance of an elementary slice of dx width in steady-state, except that under vacuum conditions, no convection occurs. In the following expressions, it is assumed that the thermal conductivity k is a constant. Indeed, platinum thermal conductivity is near 71.7 $Wm^{-1}K^{-}1$ at 273 K and 73.2 $Wm^{-1}K^{-1}$ at 600 K, with a minimum value of 71.6 near 300 K [39]. Besides, electrical resistivity ρ_{el} appears to be a constant but it is not. In the setup depicted in the next section, the input current and wire voltage are precisely measured so that the actual input power and wire resistance are known, providing the actual mean resistivity value. In our model, we then assume that the electrical resistivity ρ_{el} is an average value of the wire over its entire length, but that it depends on temperature, and which will be known as an input experimental value. The validity of this assumption is discussed in a further section. This is a key point because the simplicity of the model is required to allow the determination of the thermal contact parameters. Furthermore, it is assumed that radiation remains negligible due to low level of temperature, typically below 250°C, so that the longitudinal temperature distribution is governed by the differential equation:

$$ks\frac{d^2\theta}{dx^2}dx + \frac{\rho_{el}i^2}{s}dx = 0 \qquad (3)$$

whose general solution is: $\theta = -\frac{\rho_{el}i^2}{2ks^2}x^2 + Ax + B$

At the extremity of the wire, the condition gives for x = L:

$$\theta = 0 \quad \Leftrightarrow \quad 0 = -\frac{\rho_{el}i^2}{2ks^2}L^2 + AL + B \qquad (4)$$

At the origin x = 0, the thermocouple tip contact occurs: $2ks\frac{d\theta}{dx}\Big|_{x=0} = g\theta(0)$ (5)

$$\Leftrightarrow \quad 2ksA = gB \quad \text{and} \quad B = 2\frac{ks}{g}A$$

This leads to: $A = \frac{\rho_{el}i^2}{2ks^2}L^2\frac{g}{gL+2ks}$ and $B = \frac{\rho_{el}i^2}{2ks^2}L^2\frac{2ks}{gL+2ks}$

Finally: $\theta = \frac{\rho_{el}i^2}{2ks^2}\left(L^2\frac{gx+2ks}{gL+2ks} - x^2\right)$ (6)

For convenience, it is useful to simplify by introducing two terms:

$P = \frac{\rho_{el}L}{s}i^2$: the Joule effect internal source power (W) along the half-length L, in which the temperature dependence of resistivity ρ_{el} is taken into account since this power is an input experimental data.

$G = \frac{ks}{L}$: the internal wire thermal conductance ($W.K^{-1}$).

Then the solution is reduced to: $\theta = \frac{P}{2G}\left(g\frac{\frac{x}{L}+2G}{g+2G} - \left(\frac{x}{L}\right)^2\right)$ (7)

The central temperature where the thermocouple junction is put in contact gives:

$$\theta(0) = \frac{P}{g+2G} = \theta_c^0 \qquad (8)$$

Without contact, it simplifies with g = 0: $\theta(0) = \frac{P}{2G} = \theta_{nc}^0$ (9)

Suffix « c » means "contact" and « nc » means "no contact", and exponent "0" for the location x.

Wire electrical resistivity depends on the temperature through its temperature coefficient of resistance (TCR) α, whose value has been calibrated in oven, confirming the platinum value of 0.003858 K^{-1}.

As a result, measuring the supplied voltage and current directly provides the input power P and the wire electrical resistance R_w which relies on the mean wire temperature $\bar{\theta}$ using the classical relation:

$$R_w = R_0(1 + \alpha\bar{\theta}) \qquad (10)$$

The mean wire temperature is obtained by integrating the temperature distribution:

$$\bar{\theta} = \frac{1}{L}\int_0^L \theta\, dx = \frac{P}{12G}\,\frac{g+8G}{g+2G} \qquad (11)$$

Without contact (g=0), this simplifies to: $\overline{\theta_{nc}} = \frac{P}{3\,G}$ (12)

This value gives direct access to the central temperature of expression (9) with:

$$\theta_{nc}^{0} = \frac{3}{2}\,\overline{\theta_{nc}} \qquad (13)$$

In addition, the contact to non-contact mean temperature ratio provides a simple relation between internal and external conductance, G and g respectively as:

$$\frac{\overline{\theta_c}}{\overline{\theta_{nc}}} = \frac{1}{4}\,\frac{g+8G}{g+2G} = \beta \qquad (14)$$

According to this simple model, all these terms are linear functions of the Joule power P that depends on two parameters: G and g. G depends on the wire nature and geometry and g is the thermal conductance due to the thermocouple contact on the wire.

5. Experimental setup

The ability to work and manipulate micro-devices under vacuum has been achieved by the adaptation of a Scanning Electron Microscope (SEM) and Focused Ion Beam (FIB) station. The so-called "µRobotex" station is based on an Auriga 60 microscope produced by Zeiss. The Auriga 60 has a 60×60×60 cm^3 vacuum chamber, on the top of which a SEM FEG column is installed. The FIB column is provided by Orsay-Physics, which is positioned at an angle of 54° from the z-axis of the SEM column, as depicted in Fig. 3.

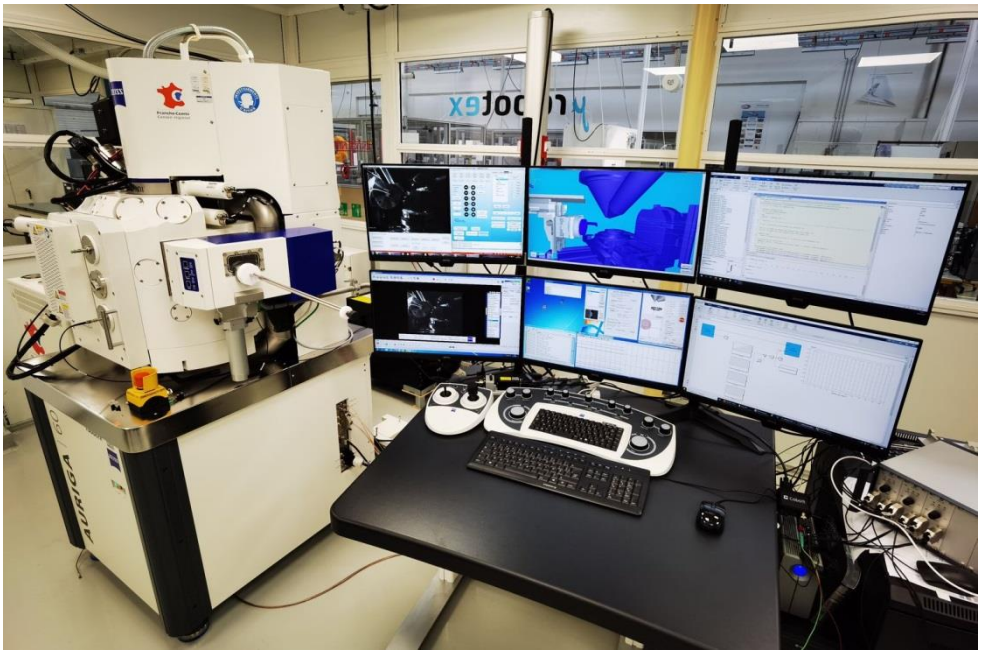

Fig. 3. Zeiss Auriga 60 SEM column system with Orsay-Physics FIB column and its HMI environment.

Furthermore, a set of six individual actuators from SmarAct has been installed in the vacuum chamber to operate as a robotic system allowing to manipulate micro-devices on all directions of space. The robotic structure is home assembled and all the robotic arms are controlled with a very high accuracy on the object location by a real time link between the control system of the SEM and the control system of the robot. The moving steps are controlled with a Human / Machine / Interface (HMI) and the softwares are home made in order to combine high accuracy of positioning and synchronization of all axes in the assembly processes. Fig. 4 depicts the internal setup of the vacuum chamber in which the 6-axis actuators system has been installed.

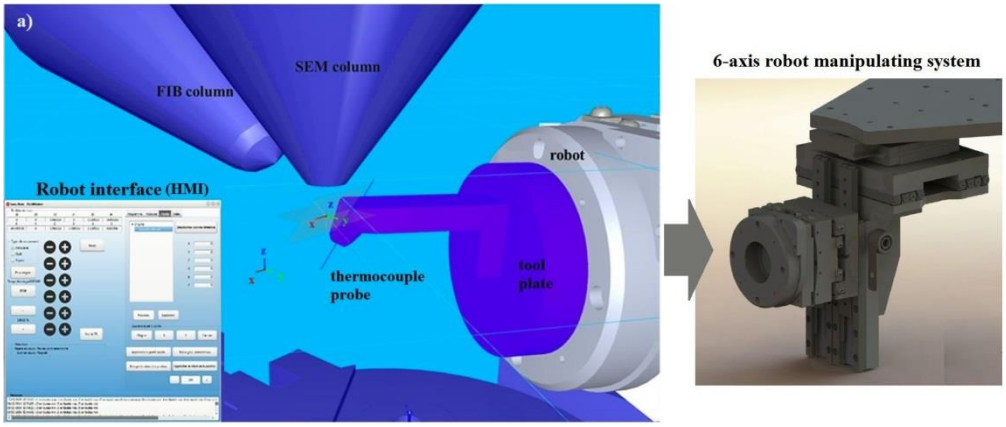

Fig. 4. HMI view of the microrobotic system and 6-axis actuators for micro-manipulation.

Different realizations have been described in previous article, using the ability of FIB to etch, weld, bend (origami technique), and the micro-robot to manipulate elements [40]. Complex structure can be obtained such as a "microhouse" [41], or integrated actuators thermally activated on optical fiber [42], or electrically heated by Joule effect [43]. In this article, the microrobot is used to manipulate the thermocouple probes in order to contact the hot wire. The experimental setup is depicted in Fig. 5 in which the used thermocouples are shown. The thermocouples cold junction reference is provided by a Pt100 sensor located on the thermocouple support.

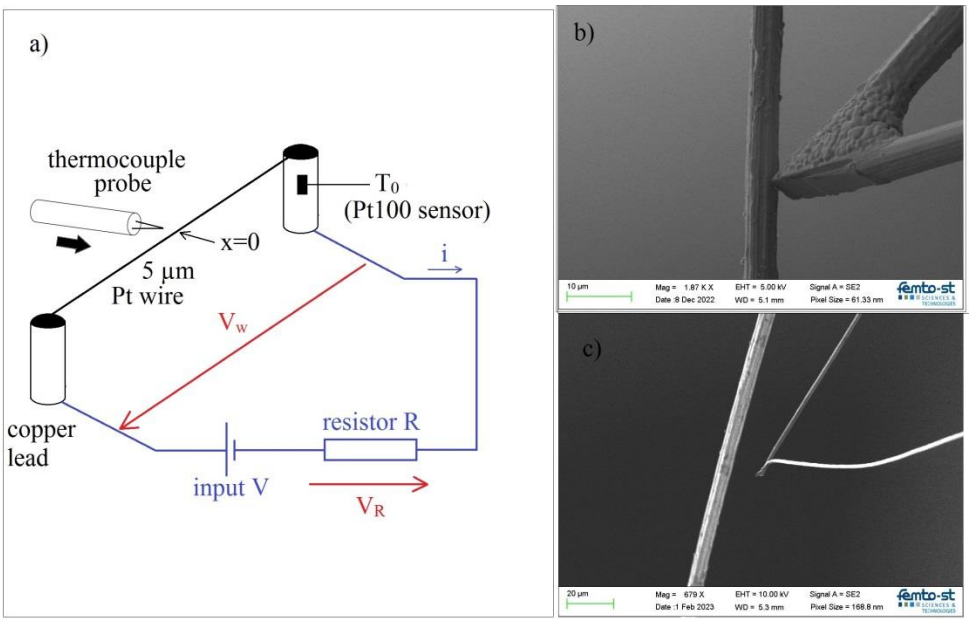

Fig. 5. a) Set-up principle; b) 5 µm thermocouple (TC5) in contact with the 5 µm platinum wire; c) 1.3 µm thermocouple (TC1) approaching.

A voltage generator supplies a current (i) into the tested wire in series with a resistor (R). Two precision voltmeters (Keithley 2000) are used to measure precisely both the current value from V_R and the wire voltage V_w. The wire resistance (R_w) and the supplied power (P) are also deduced since: $R_w = \frac{V_w}{i} = \frac{V_w}{V_R} R$ and $2P = V_w\, i = \frac{V_w}{R} V_R$ in which, accordingly to the model, P represents the half dissipated power.

The wire is welded on massive copper leads on which a Pt100 sensor is embedded in order to measure the reference temperature T_0. The microthermocouple is driven using the robot described above and depicted in Fig. 4. The contact control is made possible due to the SEM or FIB image in the vacuum chamber in order to insure the precise contact location between the thermocouple tip and the hot wire.

6. Methodology

As a first step, an oven was used to calibrate the wire by measuring precisely its electrical resistance (R_w) versus temperature. It follows that a relation is made between wire resistance and its mean temperature that correspond to the

terms: $\overline{\theta_{nc}}$ and $\overline{\theta_c}$ and its ratio β which depends on g and G only. As shown in Fig. 6, the obtained linear relationship is used to provide the mean wire temperature from its resistance. The reference value R_0 at °C is $32.502^{\pm 0.05}$ Ω and the TCR measured value is $\alpha = 3.858^{\pm 0.02} 10^{-3}$ K^{-1}.

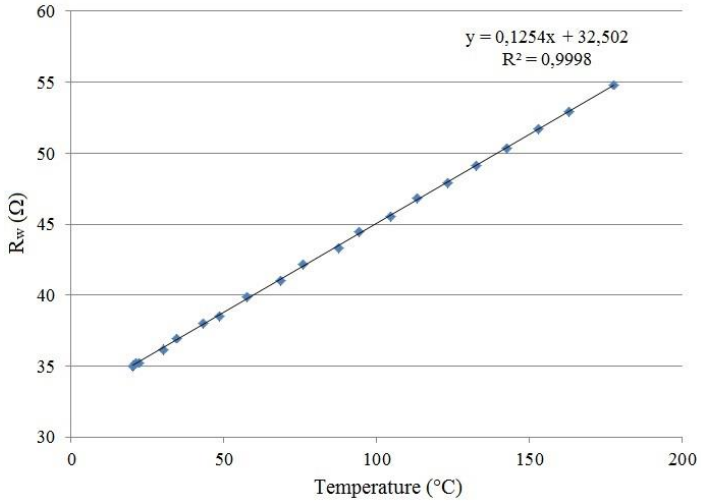

Fig. 6. Oven calibration of the 5µm diameter platinum wire: R_w versus temperature.

Then, measurements have been made in vacuum conditions of the SEM chamber without any thermocouple contact, at different input current at absolute pressure in the range 2 to 5.10^{-4} Pa. Wire resistance R_w versus the Joule power P is plotted in Fig. 7, confirming the model linearity up to a resistance value of 55 Ω typically which corresponds to 200°C approximately according to Fig. 6.

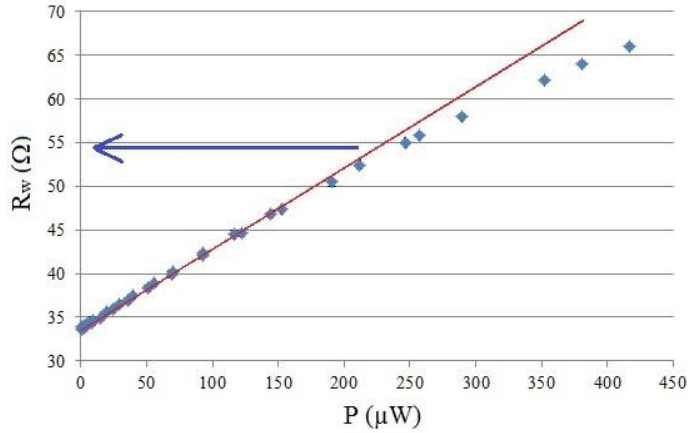

Fig. 7. Platinum wire resistance versus Joule power in vacuum showing that the linear model remains valid up to 55Ω approximately.

The deviation from linearity is mainly due to the limits of our assumptions. Firstly, the increasing difference between the assumed average electrical resistivity and its actual distribution along the wire. Secondly, the increase in radiative heat dissipation, classically proportional to T^4, and thirdly, to a lesser extent, the temperature dependence of the wire's thermal conductivity. In the following procedure, only slopes extracted from the linear domain are taken into account.
The extracted wire resistance R_w provides its mean temperature from expression (10), called $\overline{\theta_{nc}}$ without contact, which is also a linear function of Joule power P so that expression (12) gives:

$$\overline{\theta_{nc}} = \frac{P}{3\,G} = aP$$

The extracted slope "a" leads to extract G value such: $G = \frac{1}{3\,a}$

It follows that, according to expression (13), the central temperature θ_{nc}^0 can be calculated.
The mean temperature during contact is deduced from the measured resistance, also a linear function of the power P:

$$\overline{\theta_c} = bP$$

As a result, the ratio between mean temperatures is a ratio between two linear function of the power P so that expression (14) gives:

$$\frac{\overline{\theta_c}}{\overline{\theta_{nc}}} = \frac{1}{4}\,\frac{g+8G}{g+2G} = \frac{bP}{aP} = \frac{b}{a} = \beta$$

This provides the value of the contact conductance: $g = 8G\ \frac{1-\beta}{4\beta-1}$

The thermal contact described in Fig. 2 shows that the heat power Q that flows through the thermocouple in contact with the hot wire can be calculated using the contact condition of expression (5):

$$Q = g(T_m - T_0) = g\ \theta_c^0$$

And expression (8) so that: $Q = \frac{g}{g+2G} P$

This heat flow is related to different thermal resistance given in expression (1) so that:

$$Q = \frac{\theta_{nc}^0}{R_m+R_c+R_e} = \frac{\theta_c^0-\theta_p}{R_c} = \frac{\theta_p}{R_e} = \frac{\theta_{nc}^0-\theta_c^0}{R_m}$$

θ_p is given by the thermocouple probe, then:

$$R_e = \frac{\theta_p}{Q} = \frac{(g+2G)\theta_p}{gP} \quad ; \quad R_c = \frac{\theta_c^0-\theta_p}{Q} = \frac{P-(g+2G)\theta_p}{gP} \quad \text{and} \quad R_m = \frac{\theta_{nc}^0-\theta_c^0}{Q} = \frac{1}{2G} \qquad (15)$$

Both numerator and denominator are linear function of P, the ratio between each slope allows to extract each thermal resistances.

7. Results and discussion

7.1 Model validity and uncertainties

The extraction of experimental quantities remains possible as long as the model that describes the wire behaviour is simple enough but valid as well. As shown in Fig. 7, the linearity has been observed up to input power of about 200 µW where the wire reaches 55 Ω approximately. However, if platinum thermal conductivity has no significant effect, electrical resistivity is strongly dependent on temperature and may disturb the temperature distribution along the wire that is considered as a parabola [44]. In the following, expression (6) has been compared to a numerical resolution performed by finite difference method, in which temperature dependence of both thermal conductivity and electrical resistivity has been taken into account. In addition, radiative heat transfer has been considered, assuming a mean platinum emissivity of 0.12. A wire of 3.1 mm half-length L discretized in 175 slices was considered. In expression (6), platinum thermal conductivity was taken as 73 $Wm^{-1}K^{-1}$, and the electrical resistivity as a mean value for the wire but temperature corrected. Data on platinum thermal conductivity and electrical resistivity are from reference 39 and 44 respectively. The wire temperature distribution is shown in Fig. 8 for a power input of 200 µW.

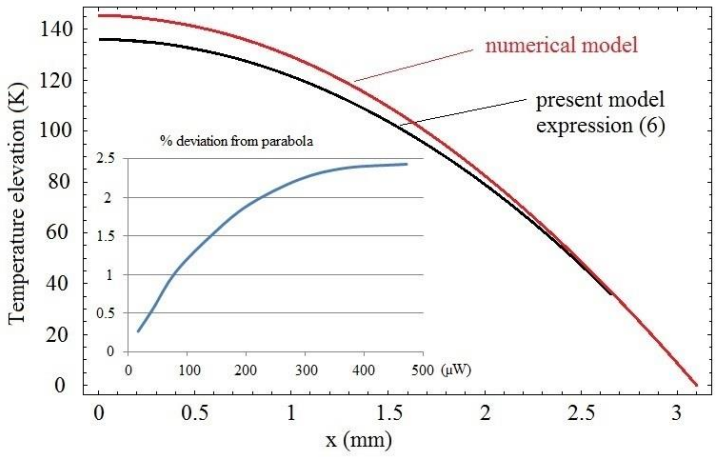

Fig. 8. Temperature distribution along the wire at a power P of 200 µW. Comparison between present model and numerical simulation. Deviation from parabolic shape calculated on the 3/2 ratio between maximum and mean temperatures in %.

One can notice that even if the shape of the numerical model is no longer parabolic, the deviation is nevertheless small enough for the 3/2 ratio between the temperature at the centre and the mean value to be less than 2% when the power is under 200 µW. From these two models, the electrical resistance of the wire can also be calculated. The result is depicted in Fig.9 in which measurement points of Fig. 7 are also plotted. The slopes are slightly different and measurements points are well fitted by both models up to 200 µW.

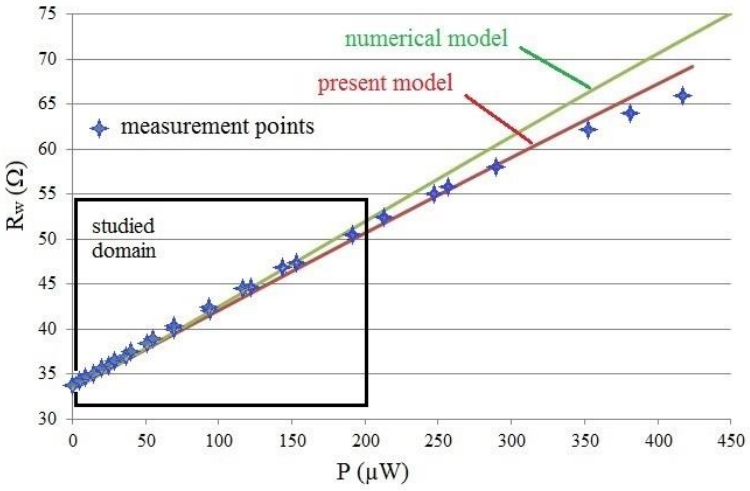

Fig. 9. Comparison of measured wire resistance with present model and numerical simulation.

As a consequence, we consider that the deviation between our simple model and numerical one remains in the range of measurement uncertainties as long the studied domain stays below 200 µW. Experimental data calculations described in the "methodology" section rely on extracted slopes that fit measurement points in this low power range for which linearity is such that R-squared coefficients are higher than 0.999 and P-values equal to zero. From these slopes, uncertainties that affect calculated values can be estimated. For this, we have considered that the relative uncertainty of high precision multimeters that provides voltage and resistance values, is taken as 10^{-3}. Furthermore, absolute uncertainty of a S type thermocouple equals 0.5 degree. Standard polynomial conversion rule is used to convert Seebeck voltage to temperature elevation. The temperature resolution corresponds to the multimeter accuracy for which the minimum temperature change is 0.2-0.3 degree. Table 1 presents a summary of the obtained relative uncertainties.

Table1: calculated propagated relative uncertainties on the different extracted terms.

Values in %	$\frac{\delta P}{P}$	$\frac{\delta R_w}{R_w}$	$\frac{\delta \bar{\theta}}{\bar{\theta}}$	$\frac{\delta G}{G}$	$\frac{\delta \beta}{\beta}$	$\frac{\delta g}{g}$	$\frac{\delta Q}{Q}$	$\frac{\delta R_m}{R_m}$	$\frac{\delta R_e}{R_e}$	$\frac{\delta R_c}{R_c}$	$\frac{\delta \tau}{\tau}$
TC5	0.22	0.17	0.6	0.64	0.85	14.6	3.9	0.64	3.9	24.3	6.3
TC1	0.22	0.17	0.6	0.64	0.85	5.1	2.7	0.64	2.7	31	4.3

7.2 Results

All the measurements points are voltages V_w and V_R obtained at different values of the supplied Joule power P, without contact and during contact of the two thermocouples. For each point, resistances are calculated and the mean temperature elevation is deduced. These temperatures are plotted in Fig. 10 for which linear fits have been extracted.

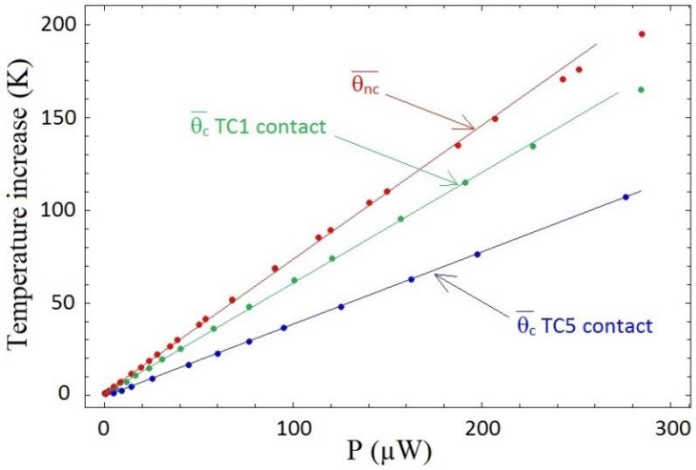

Fig. 10. Mean wire temperature before contact (red), during contact with 1.3 µm thermocouple (TC1) and 5 µm thermocouple (TC5).

The slopes of these fits provide G, β and g values for both thermocouples. As shown in Fig. 11, it follows that the central point (x=0) temperature is deduced from non-contact mean temperature using expression (13): $\theta_{nc}^{0} = T_s - T_0$
The thermocouples provide their own values after converting Seebeck voltage, giving: $\theta_p = T_p - T_0$

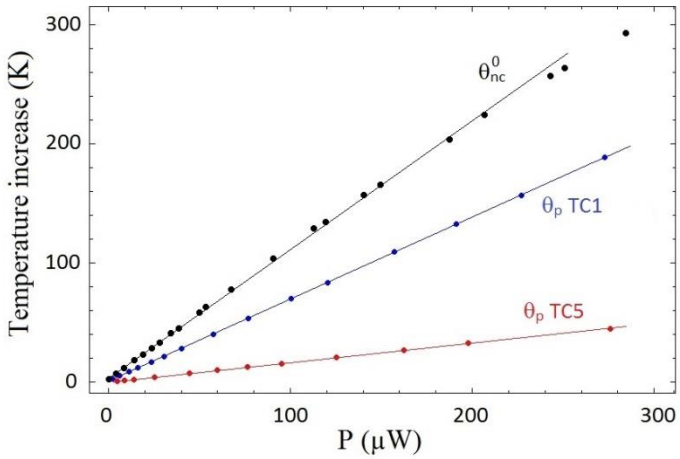

Fig. 11. Temperature elevation at point contact (x=0) before contact and thermocouple probe measurements θ_p with 1.3 µm thermocouple (TC1) and 5 µm thermocouple (TC5).

The main results are given in Table 2, from which some remarks can be made.

Table 2. Measurement results.

	G (µW.K^{-1})	β	g (µW.K^{-1})	R_m (K.W^{-1})	R_c (K.W^{-1})	R_e (K.W^{-1})	τ
TC5	$0.4512^{\pm 0.003}$	$0.5229^{\pm 0.0044}$	$1.578^{\pm 0.23}$	$1\,108\,060^{\pm 7100}$	$382\,785^{\pm 93000}$	$25.1^{\pm 1}\,10^4$	$0.1441^{\pm 0.01}$
TC1	$0.4512^{\pm 0.003}$	$0.8199^{\pm 0.007}$	$0.286^{\pm 0.015}$	$1\,108\,060^{\pm 7100}$	$626\,109^{\pm 194100}$	$286.9^{\pm 8}\,10^4$	$0.6237^{\pm 0.03}$

First, G value can be estimated since the total length can be deduced from the wire resistance R_w, the diameter and electrical resistivity of platinum, so that the half-length L equals theoretically 3.25 mm. Knowing the thermal conductivity of platinum, value of G gives 0.432 µW.K^{-1}, which confirms the experimental value.
Contact conductance g are in the usual order of magnitude of a microwatt per degree except that, without the help of convection and water meniscus around the point contact, vacuum values are inevitably lower than in ambient air conditions. This is also the case for contact resistance R_c that exhibits lower values although they highly depend on the contact strength.
External thermal resistance that characterizes the thermocouple probe R_e can be easily estimated since a wire usually acting as a fin becomes a simple wall when convection becomes negligible.
As a result, the classical expression of thermal resistance is: $R_e = \frac{l}{2kS}$; in which l is the wire length, S its cross section and k its thermal conductivity. The factor 2 comes from the fact that the thermocouple is made of two wires.
Considering a mean thermal conductivity between platinum and platinum – 10% rhodium of 60 W.m^{-1}.K^{-1}, it follows that with length of around 600 µm and 400 µm for 5 µm and 1.3 µm thermocouples respectively, one obtain values R_e of 0.254 10^6 and 2.5 10^6 K.W^{-1}, indeed very close to present measured values.
The important question remains about what would happen when the calibrated thermocouples are used to measure contact temperature on other kinds of micro-devices. Is correction factor τ still valid?
The answer is no because any other object is characterized by its own resistance value R_m and the condition of contact may also be different.
R_m value was described by authors both in macroscopic dimension and more recently at microscale. It was obtained by solving heat transfer equation in a simple contact of a flat cylinder of radius y on a homogeneous material of thermal conductivity k_s. Whatever the cylinder-to-surface contact condition, the expression of R_m is always inversely proportional to the product of the radius to the thermal conductivity, such: $R_m = \frac{A}{y\,k_s}$, A being a constant depending on the contact condition. This expression remains valid for large homogeneous object of semi-infinite depth. This is not the case in the present situation as it is confirmed by obtained expression (15) that corresponds to the wire thermal resistance under vacuum, strictly identical to the thermocouple wires R_e given above:

$$R_m = \frac{1}{2\,G} = \frac{L}{2\,k\,S}$$

This result is quite logical, thus it is possible to estimate the rate of change of R_m if the geometry of the tested device is simple enough.
Finally, the contact thermal resistance R_c can be considered as unchanged if the contact strength is not different. Likely, if one modifies the contact strength or the geometry of the contact, this could also affect R_c value as shown below.
As an example, the 5 µm thermocouple presented in Fig. 5b (TC5) has been used to measure the temperature elevation of a polyarticulated robotic gripper. It was fabricated on a tapered and metallized optical fibre tip in order to be thermally activated by the injected laser light absorption [33].
As depicted in Fig. 12, only a part of the gripper remains on the fibre tip which was damaged during testing operations. Temperature measurements were attempted in order to estimate the actual level of temperature reached at the plate location. Indeed, this question is of the most importance when designing such thermal actuator. Due to its geometry, the 5 µm diameter thermocouple exhibits two contact points with both the plate and the fibre core. As a consequence, we suppose that the contact thermal resistance R_c is decreased by a factor of two.

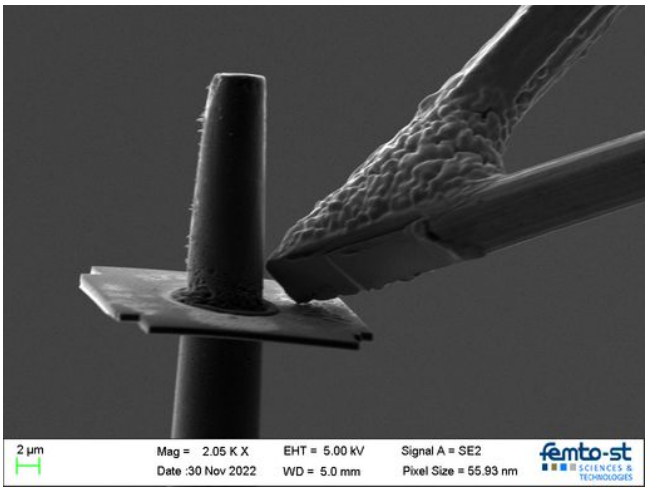

Fig. 12. TC5 thermocouple in contact with a tapered metallized optical fibre used for robotic micro-gripper.

The longitudinal thermal resistance of this fibre tip R_m can be calculated knowing its geometry and the materials. An optical fibre is quite simple in terms of geometry but the shape is not cylindrical or even simply conical and the metal deposition must be taken into account. As described in previous articles, the shape of the tapered fibre can be extracted from a binocular optical and SEM images to provide series of polynomial expressions [45,46]. The result is depicted in Fig. 13 in which a cylindrical plate has been added at a distance of 20 µm from the apex in order to represent the plate.

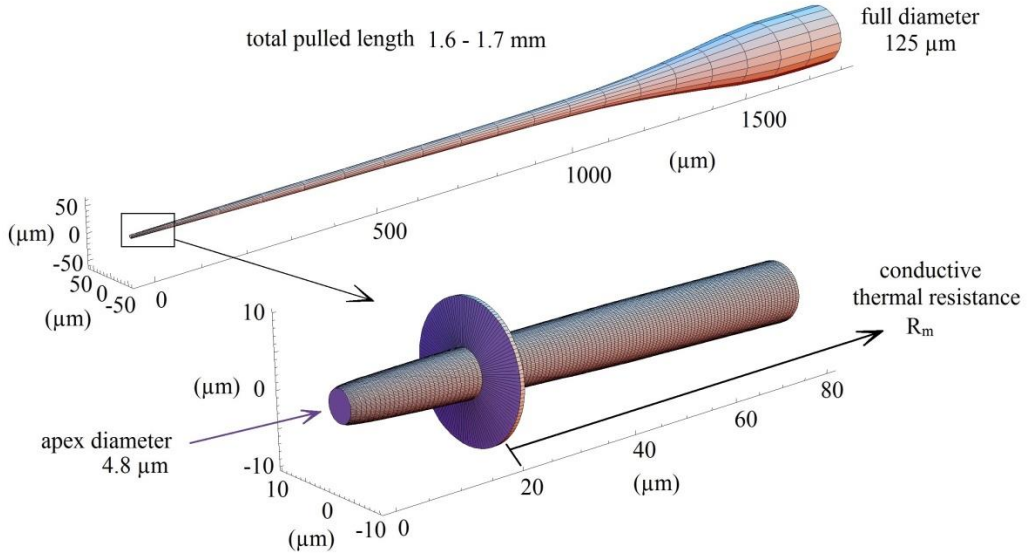

Fig. 13. Extracted fibre tip profile and discretization for the calculation of its conductive thermal resistance.

As shown in Fig. 12, the apex was cut using FIB etching so that it forms a flat extremity of 4.8 µm diameter. The metallic thin-film is a chromium layer of 50 nm thick approximately, which is enough to concentrate the light inside the

taper and evacuate the electrical charges during SEM and FIB scans. Then, the all tip is discretized into slices of sufficiently fine width for each of them to be considered as homogeneous in temperature. Next, the thermal conductivity of each element can be calculated from chromium and silica values and their proportions, and then the resulting thermal resistance over the entire length of the fibre from the point of contact to the support located 4 mm from the tip, by summing each slice thermal resistance, such: $R_m = \sum_n \left(\frac{\Delta x_n}{k_{Si}S_{Si}+k_{Cr}S_{Cr}}\right)$

For each element n of thickness Δx, silica and chromium cross sections are calculated, S_{Si} and S_{cr}, of thermal conductivities k_{Si} and k_{Cr} respectively. This simple method provides an estimation of the actual thermal resistance of the tested tip R_m. Table 2 presents the result of the different thermal resistance, compared with the previous ones of Table 1. In these results, we considered a chromium film of 50 nm thick with a thermal conductivity of 47 $Wm^{-1}K^{-1}$ (half of bulk chromium) on a silica fibre whose thermal conductivity was taken at high temperature (2 $Wm^{-1}K^{-1}$). The total fibre length is 40 mm.

Table 2. Thermal resistances and response of fibre tip compared to calibration.

TC5 measurements	R_m ($K.W^{-1}$)	R_c ($K.W^{-1}$)	R_e ($K.W^{-1}$)	τ
5 µm platinum calibration	1 108 060	382 785	251 038	0.1441
Fibre tip calculations	3 514 890	191 393	251 038	0.0634

This gives a value of R_m resistance more than three times higher than the calibration platinum wire, mainly due to the low silica thermal conductivity. Due to the double contact of the thermocouple on both the fibre and the plate, the initial contact resistance R_c has been divided by two. The external resistance R_e remains unchanged since it characterizes the thermocouple itself.

Series of temperature measurements have been performed for different laser power injected into the fibre from which modified and surface temperature values were deduced. Results are depicted in Fig. 14 in which the laser power only represents the indication values of the power supply but not the actual power that reach the fibre tip. This could explain the non-linear dependence of the temperatures versus power. Measurements have been repeated several times, and blue dots represents mean values of the TC5 thermocouple values (T_p), reaching 108°C of temperature increase at the highest point. During this contact, the green dots exhibit local fibre values underneath the contact area, then reaching a temperature increase of 194°C (T_m). According to the thermal response τ of 0.0634, the actual temperature at this point without the thermocouple is 1706°C (T_s). This seems excessive, however at this power level, when the thermocouple has been pulled of the fibre, the latter fused after some seconds. The result is shown in the top picture of Fig. 14. This confirms our estimation since fusion temperature of silica is in the range 1600-1700°C even under vacuum.

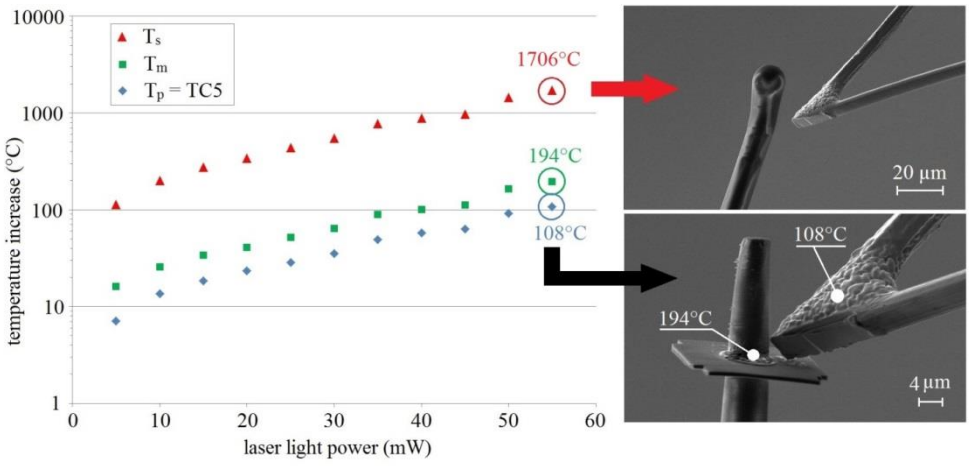

Fig. 14. Measured and deduced temperature elevation of the fibre versus laser power.

Furthermore, it is possible to confirm this result with an estimation of the thermal balance of the tip area in both cases of contact and no contact. We observed that the fused area was the extremity where the maximum light intensity is supposed to be concentrated. This part of tip fibre can be supposed at homogeneous temperature so that a thermal balance can be applied on. Let us consider this hot area as a cylinder of 10 µm length and a mean diameter of 10 µm. This part is metallized so that the emissivity remains low, typically 0.1. Without contact, the temperature of this area is 1979 K (1706°C) so that according to Stefan-Boltzmann law, the calculated net radiative power loss is 27 µW. At the same time, the conductive heat dissipated along the fibre through the estimated value of R_m gives 479 µW. The total

heat loss is then 506 µW. During contact, according to our estimation, fibre temperature is reduced to 194°C. The radiation loss is then negligible, only two conduction losses occur: in the wire thermocouple through R_e resistance at the temperature of 108°C and along the fibre core through R_m resistance. This gives 430 µW and 55 µW respectively, then a total heat loss of 485 µW, which is coherent with the losses of 506 µW without contact.

8. Conclusion

We have shown that micro-thermocouples can be used as a versatile mean for vacuum temperature measurement by contact on micro-devices especially for complex shape objects. They represent an effective mean of passive measurement but require a thorough analysis of the actual thermal conditions that fix the different values of thermal resistances that are involved in the measurements. The spatial resolution of such a technique relies on the contact area between the thermocouple tip and the surface which is on the order of 100 nm under vacuum. This is much lower than any optical technique. After having presented a calibration procedure to extract the characteristics that govern the probes behaviours, we show that it is possible, but quite difficult, to extrapolate corrections to apply on other objects. Further measurements have to be performed, notably using the smallest 1.3 µm thermocouple on different hot micro-devices, the example of metallized optical fibre tips are particularly relevant for that purpose. This will be the subject of a next article. Furthermore, the possibility to operate in active mode (CCM) using null-point method will also be explored.

References

[1] D. Teyssieux, L. Thiery and B. Cretin, Near-infrared thermography using a charge-coupled device camera: Application to microsystems, Rev. Sci. Instrum. 78, 034902 (2007), doi: 10.1063/1.2714040.

[2] D. Teyssieux, D. Briand, J. Charnay, N. F. de Rooij and B. Cretin, Dynamic and static thermal study of micromachined heaters: the advantages of visible and near-infrared thermography compared to classical methods, J. Micromech. MicroEng. 18, 065005 (2008), doi: 10.1088/0960-1317/18/6/065005.

[3] J. Christofferson and A. Shakouri, Thermoreflectance based thermal microscope, Rev. Sci. Instrum. **76** 024903 (2005), doi: 10.1063/1.1850632.

[4] G. Tessier, S. Holé, and D. Fournier, Quantitative thermal imaging by synchronous thermoreflectance with optimized illumination wavelengths, Appl. Phys. Lett. **78**, 2267 (2001), doi: 10.1063/1.1363696 .

[5] I.A. Vitkin, C. Christofides, and A. Mandelis, Photothermal reflectance investigation of processed silicon. II. Signal generation and lattice temperature dependence in ion-implanted and amorphous thin layers, J. Appl. Phys. **67**, 2822 (1990), doi: 10.1063/1.345450.

[6] C. Herzum, C. Boit, J. Kölzer, J. Otto and R. Weiland, High resolution temperature mapping of microelectronic structures using quantitative fluorescence microthermography, Microelec. J. 29, 163 (1998), doi: 10.1016/S0026-2692(97)00054-2.

[7] M. Kuball, S. Rajasingam, A. Sarua, M.J. Uren, T. Martin, B.T. Hughes, K.P. Hilton and R.S. Balmer, Measurement of temperature distribution in multifinger AlGaN/GaN heterostructure field-effect transistors using micro-Raman spectroscopy, Appl. Phys. Lett. **82** 124 (2003), doi: 10.1063/1.1534935.

[8] A. Soudi, R.D. Dawson and Y. Gu, Quantitative Heat Dissipation Characteristics in Current-Carrying GaN Nanowires Probed by Combining Scanning Thermal Microscopy and Spatially Resolved Raman Spectroscopy, ACS Nano **5**, 1, 255-262 (2011), doi: 10.1021/nn102818s.

[9] L. Marciniak, W. Piotrowski, M. Szalkowski, V. Kinzhybalo, M. Drozd, M Dramicanin, A. Bednarkiewicz, Highly sensitive luminescence nanothermometry and thermal imaging facilitated by phase transition, Chemical Engineering Journal 427 (2022) 131941, DOI: https://doi.org/10.1016/j.cej.2021.131941.

[10] A. Csendes, V. Szekely and M. Rencz, Thermal mapping with liquid crystal method, Microelec. Engin. 31, 281 (1996), doi: 10.1016/0167-9317(95)00350-9.

[11] L. Aigouy, G. Tessier, M. Mortier and B. Charlot, Scanning thermal imaging of microelectronic circuits with a fluorescent nanoprobe, Appl. Phys. Lett. **87** 184105 (2005), doi: 10.1063/1.2123384.

[12] K. E. Goodson and M. Asheghi, Near-Field Optical Thermometry, *Microscale Thermophysical Engineering*, Vol. 1 (3), 225-235 (1997), doi: 10.1080/108939597200241.

[13] M. Wyss, K. Bagani, D. Jetter, E. Marchiori, A. Vervelaki, B. Gross, J. Ridderbos, S. Gliga, C. Schönenberger, and M. Poggio, Magnetic, Thermal, and Topographic Imaging with a Nanometer-Scale SQUID-On-Lever Scanning Probe Phys. Rev. Applied **17**, 034002 (2022). DOI: https://doi.org/10.1103/PhysRevApplied.17.034002.

[14] J. Bodzenta and A. Kazmierczak-Balata, Scanning thermal microscopy and its applications for quantitative thermal measurements, J. Appl. Phys. 132, 140902 (2022), doi:10.1063/5.0091494.

[15] Yifan Li, Yuan Zhang, Yicheng Liu, Huaqing Xie & Wei Yu, A Comprehensive Review for Micro/Nanoscale Thermal Mapping Technology Based on Scanning Thermal Microscopy Journal of Thermal Science volume 31, pages976–1007 (2022); DOI : https://doi.org/10.1007/s11630-022-1654-1.

[16] S. Gomes, A. Assy and P-O. Chapuis, Scanning thermal microscopy: A review Phys. Status Solidi A 212, No. 3, 477–494 (2015) / DOI 10.1002/pssa.201400360.

[17] R.B. Dinwiddie, R.J. Pylkki and P.E. West, Thermal conductivity contrast imaging with a scanning thermal microscope, Proc. Thermal Conductivity 22, ed. T.W. Tong (Lancaster, PA:Technomics) p.668 (1994), ISBN No. 1-56676-172-7.
[18] G. Fish, O. Bouevitch, S. Kolotov, K. Lieberman, D. Palanker, I. Turovets and A. Lewis, Ultrafast response micropipette-based submicrometer thermocouple, Rev. Sci. Instrum. 66 (5), 3300 (1995), doi: 10.1063/1.1145498.
[19] A. Majumdar, J. Lai, M. Chandrachood, O. Nakabeppu, Y. Wu and Z. Shi, Thermal imaging by atomic force microscopy using thermocouple cantilever probes, Rev. Sci. Instrum. 66, 3584 (1995), doi: 10.1063/1.1145474.
[20] R. A. Secco and R. F. Tucker, Thermocouple butt-welding device, Rev. Sci. Instrum. 63, 5485 (1992), doi: 10.1063/1.1143375.
[21] L. Thiery, Thermoelectrical micro-probes. Local measurements applications, Rev. Gen. Therm. 394 (1994), 551-561, ISSN 0035-3159..
[22] Yo. Zhang, Ya. Zhang, J. Blaser, T.S. Sriram, A. Enver and R.B. Marcus, A thermal microprobe fabricated with wafer-stage processing, Rev. Sci. Instrum. 69, 2081 (1998), doi: 10.1063/1.1148902 .
[23] T. Leinhos, M. Stopka, E. Oesterschulze, Micromachined fabrication of Si cantilevers with Schottky diodes integrated in the tip, Appl. Phys. A 66, S65 (1998), doi: 10.1007/s003390051101.
[24] G. Mills, H. Zhou, A. Midha, L. Donaldson and J.M.R. Weaver, Scanning thermal microscopy using batch fabricated thermocouple probes, Appl. Phys. Lett. 72 (22), 2900 (1998), doi: 10.1063/1.121453.
[25] L. Shi, O. Kwon, A.C. Miner and A. Majumdar, Design and batch fabrication of probes for sub-100 nm scanning thermal microscopy, J. MicroElectroMechanical Sys. 10 (3), 370-378 (2001), doi: 10.1109/84.946785.
[26] L. Thiery, C. Bainier, M. Spajer, New opto-thermal probes on near-field optical fibre tips, OPTO 2002 International Conference Proceedings, 193-196, Erfurt (Germany) 14-16 mai 2002.
[27] P. Voisin, L. Thiery, G. Bröm, Exploration of the atmospheric lower layer thermal turbulences by means of microthermocouples, Eur. Phys. J. Appl. Phys., **7** (2), 177-187 (1999), doi: 10.1051/epjap:1999212.
[28] L. Thiery, N. Marini, J.P. Prenel, M. Spajer, C. Bainier and D. Courjon, Temperature profile measurements of near-field optical microscopy fiber tips by means of sub-micronic thermocouple, Int. J. Therm. Sci., **39 (4)**, 519 (2000), doi: 10.1016/S1290-0729(00)00231-3.
[29] A. Bontempi, D. Teyssieux, J.M. Friedt, L. Thiery, D. Hermelin, and P. Vairac, Photo-thermal quartz tuning fork excitation for dynamic mode atomic force microscope, Appl. Phys. Lett. 105, 154104 (2014), doi: 10.1063/1.4896784.
[30] T.P. Nguyen, L. Thiery, S. Euphrasie, E. Lemaire, S. Khan, D. Briand, L. Aigouy, S. Gomes and P. Vairac, Calibration tools for Scanning Thermal Microscopy probes used in temperature measurement mode, J Heat Transfer 141(7) 071601 (2019); HT-18-1667, doi: 10.1115/1.4043381.
[31] T.P. Nguyen, L. Thiery , S. Euphrasie , S. Gomès , B. Hay, and P. Vairac, Calibration of thermocouple-based scanning thermal microscope in active mode (2ω method), Rev. Sci. Instrum. 90, 114901 (2019), doi: 10.1063/1.5119044.
[32] B. Cassagne, G. Kirsch et J.P. Bardon, Theoretical analysis of the errors due to stray heat transfer during the measurement of a surface temperature by direct contact, Int. J. Heat Transfer , 23 (9), 1207, (1980), doi: 10.1016/0017-9310(80)90051-4.
[33] N.R. Keltner and J.V. Beck, Surface Temperature Measurement Errors, J. Heat Transf. 105 (2), 312 (1983), doi: 10.1115/1.3245580.
[34] J. Chung, K. Kim, G. Hwang, O. Kwon, S. Jung, J. Lee, J.W. Lee, G.T. Kim, Quantitative temperature measurement of an electrically heated carbon nanotube using the null-point method, Rev. Sci. Instrum. 81 (2010) 114901; doi: https://doi.org/10.1063/1.3499504.
[35] F. Menges, H. Riel, A. Stemmer and B. Gotsmann, Quantitative Thermometry of Nanoscale Hot Spots, Nano Lett. 2012, 12, 596−601, dx.doi.org/10.1021/nl203169t.
[36] F. Menges, P. Mensch, H. Schmid, H. Riel, A. Stemmer and B. Gotsmann, Temperature mapping of operating nanoscale devices by scanning probe thermometry, Nature Communications 7-10874, DOI: 10.1038/ncomms10874.
[37] J. Cha, H. Shin, O. Kwon, Vacuum null-point scanning thermal microscopy: Simultaneous quantitative nanoscale mapping of undisturbed temperature and thermal resistance, International Journal of Thermal Sciences 172 (2022) 107268, DOI: https://doi.org/10.1016/j.ijthermalsci.2021.107268.
[38] J. Zhang, P. Weng and Q. Liu, Monitoring a heatsink temperature field using Raman-based distributed temperature sensor in a vacuum and -173°C environment, Sensors 2019, 19, 4186, doi: 10.3390/s19194186.
[39] C.Y. Ho, R.W. Powell and P.E. Liley, "Thermal Conductivity of the Elements", Journal of Physical and Chemical Reference Data 1, 279 (1972); https://doi.org/10.1063/1.3253100..
[40] R. El Beainou, J.-Y. Rauch, S. Dembélé, O. Lehmann, L. Hirsinger and M. Devel, Qualitative evidence of the flexoelectric effect in a single multi-wall carbon nanotube by nanorobotic manipulation, Appl. Phys. Lett. 120, 033101 (2022), doi: 10.1063/5.0065214.
[41] Rauch J-Y, Lehmann O., Rougeot P., Abadie J. and Agnus J., Smallest microhouse in the world, assembled on the facet of an optical fiber by origami and welded in the μRobotex nanofactory, Journal of Vacuum Science & Technology A 36, 041601 (2018), doi: 10.1116/1.5020128.
[42]Y. Lei, C. Clévy, J-Y. Rauch and P. Lutz, Nanorobotics polyarticulated structure with integrated actuator at tapered optical fiber tip, MARSS, Int. Conf. Manip., Autom. And Robotics at Small Scales, Toronto, July 25-29, 2022.

[43] Benouhiba A., Wurtz L., Rauch J-Y., Agnus J., Rabenorosoa K. and Clévy C., NanoRobotic Structures with Embedded Actuation via Ion Induced Folding, Advanced Materials 33, 45, November 11 (2021), 2103371, Wiley VCH, doi: 10.1002/adma.202103371.
[44] J.W. Arblaster, Selected Electrical Resistivity Values for the Platinum Group of Metals Part I: Palladium and Platinum, Johnson Matthey Technol. Rev., 2015, 59, (3), 174–181; http://dx.doi.org/10.1595/205651315X688091.
[45] L. Thiery, N. Marini, C. Bainier and D. Charraut, Distribution of light density inside metal coated micrometer-size optical tapers, Optical Engineering, 40 (6), 1010-1015 (2001), doi: 10.1117/1.1369597.
[46] L. Thiery and N. Marini, Thermal behaviour modelling of tapered optical fiber for scanning near-field microscopy, Ultramicroscopy 94 (1), 49 (2003), doi: 10.1016/S0304-3991(02)00200-0.